Journal of Cluster Science, Vol. 16, No. 2, June 2005 (© 2005)
DOI: 10.1007/s10876-005-4547-z

Synthesis of Pt–Mo/Carbon Nanocomposites from Single-Source Molecular Precursors: A (1:1) PtMo/C PEMFC Anode Catalyst Exhibiting CO Tolerance*

Krzysztof C. Kwiatkowski,[1] Stephen B. Milne,[1] Sanjeev Mukerjee,[2] C. M. Lukehart[1,3]

Received November 11, 2004

Reactive, thermal degradation of $py_2Pt[MoCp(CO)_3]_2$, $(Me)(cod)PtMoCp(CO)_3$, or$\{Pt_3(dppm)_3(CO)[Mo(Cp)]\}[BPh_4]$/Vulcan carbon powder composites affords Pt–Mo/carbon nanocomposites containing metal nanoparticles of approximate compositions, $PtMo_2$, PtMo, or Pt_3Mo, widely dispersed on the carbon support. Total metal loadings range from 29–58 wt%. When tested as an anode electrocatalyst in a PEM fuel cell using either pure H_2 or H_2 containing 100 ppm CO as a fuel, the PtMo/carbon nanocomposite exhibits CO tolerance.

KEY WORDS: Pt–Mo clusters; electrocatalysts; CO tolerance.

INTRODUCTION

There is recognized need within the proton-exchange-membrane (PEM) and direct-methanol fuel cell (DMFC) research communities for the development of improved electrocatalysts [1]. In PEMFCs and DMFCs, metal alloy electrocatalysts exhibit excellent performance and continue to be catalyst compositions of great interest. Metal alloy nanoparticles are prepared using a variety of physical or chemical synthesis methodologies including reductive

* Dedicated to F. A. Cotton on the occasion of his 75th birthday.

[1] Department of Chemistry, Vanderbilt University, Nashville, Tennessee, 37235, USA.
[2] Department of Chemistry, Northeastern, University, 360 Huntington Avenue, Boston, Massachusetts, 02115, USA.
[3] To whom correspondence should be addressed. E-mail: charles.m.lukehart@vanderbilt.edu.

co-precipitation of dissolved metal ions and chemical reduction of preformed mixed-metal salts as the most common routes. Carbon-supported metal alloy nanocomposites are attractive catalysts for low-temperature fuel cell applications to minimize precious metal cost.

As part of an on-going investigation to develop alternative synthesis strategies for the preparation of metal alloy/carbon nanocomposites that exhibit electrocatalytic performance, we are exploring the use of single-source molecular precursors as sources of metal. Reactive, thermal degradation of precursor/carbon composites under appropriate conditions affords metal alloy/carbon nanocomposites having metal stoichiometries close to that of the corresponding precursor without incurring gross phase separation of the metal components. Ideally, precursor compounds should be readily prepared and easily handled under ambient conditions. The resulting metal alloy/carbon nanocomposites should be available in gram-scale quantities.

We have recently prepared Pt–Ru/carbon nanocomposites having an alloy composition of ca. Pt_1Ru_1 using five different non-cluster (1:1)-Pt,Ru bimetallic precursors [2]. When tested as anode electrocatalysts in DMFCs, these nanocomposites give cell performances essentially equivalent to that measured under identical testing conditions for a commercial, unsupported Pt_1Ru_1 colloidal catalyst. A Pt–Ru/graphitic carbon nanofiber nanocomposite prepared by this method reproducibly exhibits significantly enhanced performance relative to this same standard.

Such promising results have led us to extend the scope of this synthesis strategy to the preparation of Pt–Mo/carbon nanocomposites as potential CO-tolerant PEMFC anode electrocatalysts. Discovery of CO-tolerant anode catalysts is crucial to the development of high-performance H_2/O_2 PEM fuel cells operating with reformate fuels contaminated by CO [1c, 3]. While Pt catalysts are rapidly poisoned by CO, Pt–Mo catalysts, particularly those having Pt-rich compositions, exhibit various degrees of CO tolerance [4].

We now report the preparation and characterization of three Pt–Mo/Vulcan carbon nanocomposites having Pt–Mo atomic compositions of ca. $PtMo_2$, PtMo, or Pt_3Mo using $py_2Pt[MoCp(CO)_3]_2$, (Me)(cod)Pt-$MoCp(CO)_3$, or$\{Pt_3(dppm)_3(CO)[Mo(Cp)]\}[BPh_4]$, respectively, as single-source molecular precursors of metal nanoparticles. The PtMo/carbon nanocomposite exhibits excellent air stability and can be obtained from a readily available precursor. This nanocomposite performs as a PEM electrooxidation catalyst when using either pure H_2 or H_2 containing 100 ppm CO as fuel. Due to the relatively low cost and high abundance of Mo, further investigation of the electrocatalytic performance of

PtMo/carbon nanocomposites prepared by this synthesis strategy appears to be warranted.

EXPERIMENTAL

Reagents and Methods

Nitrogen gas used in the following reactions was passed through a drying column containing Drierite ($CaSO_4$) prior to use. Evaporations on a steam bath were conducted in the open air. All solvents were purchased from Fisher Chemical Company, Inc., as reagent grade and were distilled prior to use. Tetrahydrofuran was distilled from Na/K alloy in the presence of benzophenone. Cyclopentadienylmolybdenumtricarbonyl dimer, $[(\eta\text{-}C_5H_5)Mo(\text{-}CO)_3]_2$, dichloro(1,5-cyclooctadiene)platinum(II), $Pt(cod)Cl_2$, and potassium tetrachloroplatinate, $K_2[PtCl_4]$, were purchased from Strem Chemical Company, Inc. Pyridine, ammonium hexafluorophosphate and trifluoroacetic acid were purchased from Aldrich Chemical Company, Inc. Celite 545 (diatomaceous earth), decolorizing carbon (Norit), potassium iodide, and sodium tetraphenylborate were purchased from Fisher Chemical Company, Inc. Hydrochloric acid and Silica Gel 60 were purchased from EM Science Chemical Company, Inc. Vulcan Carbon XC-72R was purchased from Cabot Corporation. Combax alumina-silicate combustion boats used to prepare the nanocomposite materials were purchased from Fisher Scientific. Copper grids of 3-mm diameter coated with amorphous holey carbon support were purchased from Ted Pella, Inc., and were used for TEM analysis of the carbon nanocomposites. Bulk chemical elemental analyses were performed by Galbraith Laboratories, Inc., Knoxville, TN. The following starting materials and complexes were prepared by literature methods or with only minor modification of literature methods cited: $[Pt_3(dppm)_3(CO)][CF_3CO_2]_2$ [5], $[Pt_3(dppm)_3(CO)][PF_6]_2$ [5], $Na[MoCp(CO)_3]$ [6], $Pt(cod)Cl_2$ [7], $Pt(cod)I_2$,[7] $Pt(cod)Me_2$ [7], Pt(cod)(Me)Cl [7], trans-$Ptpy_2Cl_2$ [8], (cod)(Me)-$PtMoCp(CO)_3$, **2a** [9], and trans-$(py)_2Pt[MoCp(CO)_3]_2$, **1a** [10], where py = pyridine, dppm = bis(diphenylphosphino)methane, Cp = $\eta\text{-}C_5H_5$ and cod = 1,5-cyclooctadiene. Preparations of known complexes using modifications of literature procedures are included in detail.

Nuclear magnetic resonance (NMR) spectra were obtained on a Bruker AC300 Fourier Transform spectrometer operating at 300 MHz, using the deuterium signal of the solvent as the internal lock frequency. ^1H chemical shifts were referenced to TMS, and ^{31}P-NMR chemical shifts were referenced to 80% H_3PO_4.

Nanocomposite materials were characterized on a Philips CM20T transmission electron microscope (TEM) operating at 200 kV and equipped

with an EDS detector. Samples for TEM were prepared by putting one drop of a suspension of fine-powdered composite material in methylene chloride onto a 3-mm diameter holey carbon copper grid followed by evaporation of the solvent. Particle size distributions were obtained from standard bright-field (BF) images. Electron diffraction ring patterns were obtained using selected area diffraction (SAD). X-ray energy dispersive spectroscopy (EDS) was used for qualitative and semi-quantitative analysis of elements heavier than F on the micron scale. Copper x-ray emission from the TEM sample-grid holder is observed in all recorded EDS spectra.

X-ray diffraction (XRD) scans were obtained using a Scintag X_1 Advanced Diffraction System equipped with a solid-state Peltier detector, a high-temperature unit integrated with a sample holder, standard room-temperature sample holder, and a computer controlled gas delivery system. A copper x-ray tube was used as the source of radiation. Samples for a room-temperature attachment were prepared by filling a sample well on a plastic plate. Samples for high temperature XRD study were prepared by covering dropwise a zero-background slide of Si(510) with a suspension of a powdered sample in pentane and allowing the pentane to evaporate leaving a "smear" of the sample on the silicon plate. XRD scans used for particle-size determinations were corrected for background scattering and stripped of the $K_{\alpha 2}$ portion of the diffracted intensity using the DMSNT software provided by Scintag. Observed peaks were fitted with a profile function to extract the full-width-at-half-maximum (FWHM) values. Average crystallite size was calculated from Scherrer's equation ($L = K\lambda/\beta\cos\theta_B$) assuming that peak broadening arises from size effects only, where λ is the wavelength of x-rays used, β is the full-width-at-half-maximum in radians measured on the 2θ scale, θ_B is the Bragg angle for the observed *hkl* peak, and K is a constant equal to 0.9 for volume averaged crystallite dimension perpendicular to the *hkl* diffraction plane [11]. Two semi-exhaustive trial-and-error powder indexing programs for all symmetries, TREOR [12] and DICVOL91 [13], were used to auto-index the XRD scans and to calculate cell constants.

Preparation of a Carbon-supported Nanocomposite Containing 58 wt% $PtMo_2$,1b

Vulcan carbon (0.14 g) was added to a solution of trans-$py_2Pt[MoCp(CO)_3]_2$, **1a**, (0.44 g) in 80 mL of DMSO. The resulting suspension was stirred for 12 h. Deposition of the precursor complex onto the carbon support was completed by removal of the liquid phase under reduced pressure. After removal of the DMSO, the precursor/carbon composite was dried under reduced pressure at 100 °C for 4 h. Preliminary high temperature XRD experiments were conducted on a small amount of precursor/carbon

composite to optimize the heating conditions to be used for a bulk-scale synthesis using a tube furnace for thermal treatments. The precursor/carbon composite was placed into a tube furnace in a porcelain boat and was treated thermally under the following conditions: 25 to 280 °C (15 °C/min) under air; 280 °C 10 min under N_2, 280–650 °C (15 °C/min) under getter gas (90/10 N_2/H_2 mixture); 650 °C 10 min getter gas, annealed under N_2 gas at 650 °C for 50 min, after which time the sample was cooled to room temperature under N_2. Elemental analysis results obtained for nanocomposite **1b**: C, 31.81; H, < 0.5; Pt, 29.32; Mo, 28.90. The calculated Pt:Mo atomic ratio is 0.50.

Preparation of a Carbon-supported Nanocomposite Containing 43 wt% PtMo, 2b

Vulcan carbon (93.9 mg) was added to a solution of (Me)(cod)-$PtMoCp(CO)_3$, **2a**, (94.2 mg) in 30 mL of methylene chloride. The resulting suspension was stirred for 30 min. Deposition of any non-adsorbed precursor onto the carbon support was completed by removal of the liquid phase under reduced pressure. Preliminary high temperature XRD experiments were conducted on a small sample of precursor/carbon composite to optimize heating conditions to be used on a bulk-scale preparation using a tube furnace for thermal treatments. The resulting precursor/carbon composite was placed into a tube furnace in a porcelain boat and was treated thermally under the following conditions: 25–280 °C (15 °C/min) under air; 280 °C 10 min under N_2; 280–650 °C (15 °C/min) under getter gas (90/10 N_2/H_2 mixture); then the furnace was cooled to room temperature under N_2. The carbon nanocomposite was transferred to a flask containing a solution of an additional 86.2 mg of the precursor complex, **1a**, dissolved in 30 mL of methylene chloride and was stirred for 30 min. After evaporation of the liquid phase, the resulting composite was placed into a tube furnace and was treated thermally under the following conditions: 25–280 °C (15 °C/min) under air; 280 °C 10 min under N_2; 280–650 °C (15 °C/min) under getter gas; annealed under N_2 at 650 °C for 1 h after which time the sample was cooled to room temperature under N_2 gas. Elemental analysis results obtained for nanocomposite **2b** were as follows: C, 39.44; H, < 0.5; Pt, 27.48; Mo, 15.87. The calculated Pt:Mo atomic ratio is 0.9.

Preparation of (μ_3-carbonyl)tris[μ-bis(diphenylphosphino)methane]-triangulo-triplatinum(2 +) tetraphenylborate

Crude $[Pt_3(\mu_3\text{-}CO)(\mu\text{-dppm})_3][CF_3CO_2]_2$ (1.25 g, 0.63 mmol) was dissolved in 20 mL of methanol and excess sodium tetraphenylborate (1.22 g, 3.56 mmol) was added. Upon addition of the $Na[BPh_4]$ a orange

precipitate formed immediately. This product was isolated by filtration, was washed with methanol (1 mL), and was dried under reduced pressure. Orange crystals were redissolved in 20 mL of acetone and were precipitated by the addition of 20 mL of methanol. The supernatant liquid was decanted, and the crystals were washed with methanol yielding 0.89 g (56%) of $[Pt_3(\mu_3\text{-}CO)(\mu\text{-dppm})_3][BPh_4]_2$.

Preparation of {μ_3-[(η-cyclopentadienyl)molybdenum]}{(μ_3-carbonyl)tris[μ-bis(diphenylphosphino)methane]-triangulo-triplatinum(1 +)} hexafluorophosphate, 3a′

$[CpMo(CO)_3]_2$ (0.25 g, 0.51 mmol) was added to a mixture of Na/Hg (prepared by dissolving ca. 2 g Na in 7 mL of Hg) and 10 mL of THF. The reaction mixture was allowed to stir under N_2 for 3 h, during which time the reaction solution changed from red to olive green. The olive solution was filtered through Celite into another Schlenk flask purged with N_2 containing $[Pt_3(CO)(dppm)_3][PF_6]_2$ (0.201 g, 0.097 mmol) in 30 mL of THF causing the color to turn deep red. The reaction mixture was stirred for 24 h, and then the solvent was removed under reduced pressure. The residue was redissolved in about 3 mL of THF and was purified on a silica column packed in methylene chloride. The product was eluted with methylene chloride as a dark red band and was crystallized from methylene chloride/pentane solution to give 0.11 g (53%) of $\{Pt_3(dppm)_3[Mo(Cp)](CO)\}[PF_6]$, **3a′**: ^{1}H-NMR ($CDCl_3$) δ 7.5–6.9 (60H, m, dppm Ph), 5.42 (5H, s, Cp); ^{31}P_NMR ($CDCl_3$) δ 51.4 (heptet, PF_6^-, $J^2FF = 713$ Hz), −8.3 (m, dppm, $J^1PtP = 3734$ Hz, $J^3PtP = 196$ Hz). Anal. Calcd. for $C_{81}H_{71}F_6OMoP_7Pt_3$: C, 46.94; H, 3.45. Found: C, 47.21; H, 3.81.

Preparation of {μ_3-[(η-cyclopentadienyl)molybdenum]}(μ_3-carbonyl) tris[μ-bis(diphenylphosphino)methane]-triangulo-triplatinum(1 +) tetraphenylborate, 3a

A solution containing 99.2 mg (0.20 mmol) of $[CpMo(CO)_3]_2$ in 30 mL of THF was transferred under a N_2 purge to a Schlenk tube containing Na/Hg amalgam (1 g Na in 6 mL Hg). The solution was stirred for 3 h and then was filtered through a glass pouring spout packed with Celite trapped between two pieces of glass wool directly into a second Schlenk vessel containing 500 mg (0.19 mmol) of $[Pt_3(dppm)_3(CO)][BPh_4]_2$ dissolved in 30 mL of THF. After the reaction solution had stirred for approximately 24 h, the solvent was removed under reduced pressure. A silica gel column (60–200 mesh) was prepared in air using methylene chloride, and the dark red to purple colored sample was added to the column in a minimum amount of

methylene chloride. A deep red band was eluted from the column with CH_2Cl_2. The solid obtained from this band was recrystallized from CH_2Cl_2/pentane to give 287 mg (64%) of a dark red solid of$\{Pt_3(dppm)_3[Mo(Cp)](CO)\}[BPh_4]$, **3a**: ^{1}H-NMR ($CDCl_3$) δ 7.5–7.3 (m, BPh_4), 7.2–6.8 (60H, m, dppm Ph), 4.79 (5H, s, Cp). Anal. Calcd. for $C_{105}H_{91}BMoOP_6Pt_3$: C, 56.13; H, 4.08. Found: C, 55.67; H, 4.11.

Preparation of a Carbon-supported Nanocomposite Containing 29 wt% of Pt_3 Mo, 3b

The tetranuclear cluster precursor complex, $\{Pt_3(dppm)_3[Mo(Cp)](CO)\}$ $[BPh_4]$, **3a**, (0.39 g), was dissolved in 35 mL of methylene chloride. The resulting solution was stirred for 18 h with 0.25 g of Vulcan carbon powder. Deposition of the precursor onto carbon support was completed by removal of the liquid phase under reduced pressure. Preliminary high-temperature XRD experiments were conducted on a small sample of precursor/carbon composite to optimize heating conditions for bulk-scale preparations using a tube furnace for thermal treatments. The precursor/carbon composite was placed into a tube furnace in a porcelain boat and was treated thermally under the following conditions: 25–350 °C (15 °C/min) under air; 350 °C 10 min under N_2; 350–650 °C (15 °C/min) under getter gas (90/10 N_2/H_2 mixture); 650 °C 10 min under N_2; then cooling to room temperature under N_2. The carbon nanocomposite was transferred to a flask containing a solution of an additional 0.47 g of the precursor complex **3a** dissolved in 35 mL of methylene chloride and was stirred for 18 h. After removal of the liquid phase at reduced pressure, the resulting composite was placed into a tube furnace and was treated thermally under the following conditions: 25–350 °C (15 °C/ min) under air; 350 °C 10 min under N_2; 350–650 °C (15 °C/min) under getter gas (90/10 N_2/H_2 mixture); anneal under N_2 gas at 650 °C for 1 h, after which time the sample was cooled to room temperature, heated (30 °C/min) to 350 °C under air and cooled to room temperature under a N_2 purge giving the Pt_3Mo/carbon nanocomposite **3b**. Elemental analysis results obtained for nanocomposite **3b** were as follows: C, 31.13; H, 1.37; P, 6.91; Pt, 25.08; Mo, 4.23. The calculated Pt:Mo atomic ratio was 2.94.

Full-Profile Rietveld Refinement of Face-Centered-Cubic Pt–Mo Alloy Phases Present in the $PtMo_2$, PtMo, and Pt_3Mo/Vulcan Carbon Nanocomposites 1b, 2b, and 3b

The structures of the Pt–Mo crystalline nanoparticulate phase of nanocomposites **1b**, **2b**, and **3b** were confirmed by full pattern profile

refinement of the corresponding powder XRD patterns using the Rietveld method and the software program FULLPROF [14]. XRD scans were obtained on the instrumentation described above using Cu Kα radiation (Cu Kα wavelength = 1.540562 Å; Cu Kβ wavelength = 1.544390 Å) with a step size of 0.050° in 2θ and a count time of 4.0 s. Samples for room-temperature XRD scans were prepared by filling the sample well on a standard plastic plate sample holder. Scans were collected using the DMSNT software provided by Scintag. Each XRD scan was exported in GSAS format, and the resulting file was edited. Minor corrections were required to prepare exported files for FULLPROF Intensity Data File format and were limited to the removal of a second "empty" line, putting extra spaces between scan parameters in the first line, and changing the file extension to ".dat".

Input data/parameters used in the full-profile Rietveld refinement are listed in Table I along with values of output parameters following successful refinement. The crystal structure of each Pt–Mo phase was assumed to be a fully disordered face-centered-cubic unit cell having Fm3m symmetry with a Pt:Mo atomic ratio of the corresponding precursor. The background was refined using Fourier filtering. The following FULLPROF parameters were refined: cell constant, zero shift, scale factor, profile parameters (**U, V, W**), asymmetry parameter (η), and overall isotropic thermal parameter ($\mathbf{B_{iso(ov.)}}$). All atoms were treated as having isotropic thermal motion. Due to the high symmetry of the cell, which resulted in a limited number of observed reflections, only up to 6 parameters could be refined simultaneously. Tabulations of the observed, calculated, difference peak intensities, and Figures showing observed, calculated, and difference diffraction patterns for each cell refined are available from the author.

PEM Fuel Cell Measurements

The PtMo/Vulcan nanocomposite **2b** was evaluated for CO-tolerance as a hydrogen oxidation electrocatalyst in a working H_2/O_2 PEMFC. Steady-state polarization measurements on CO tolerance were carried out in a fuel cell test station using a cell fixture for a 5-cm^2 MEA that allowed for both single and half-cell polarization measurements. Methods of fabrication of the anode and cathode electrodes and the corresponding MEAs have been described in detail elsewhere [15]. Performance of H_2/CO [0 ppm or 100 ppm]//O_2 fuel cells were measured at 85 °C using a Nafion 115 membrane. Anode and cathode pressures were 16/11 psig, respectively, with humidification temperatures of 100/90 °C. PtMo/Vulcan carbon nanocomposite **2b** served as the anode catalyst at a loading of 0.4 mg total metal/cm^2. Pt/C [E-TEK, Inc.] served as the cathode catalyst at a loading of

Table I. Input Data and Refinement Results of Full-Profile Rietveld Refinement of the XRD Patterns of Pt–Mo/Vulcan Carbon Nanocomposites **1b** ($PtMo_2$), **2b** (PtMo), and 3b (Pt_3Mo)

	1b	**2b**	**3b**
Input Item/Parameter			
Refinement type	Global	Global	Global
Input data type	Free format	Free format	Free format
Angular range (° 2θ)	30–130	30–135	30–130
Step size (° 2θ)	0.05	0.05	0.05
Space group; Z	Fm3m; 4	Fm3m; 4	Fm3m; 4
Cell parameter (Å)	3.9166	3.923	3.9123
Pt position (occupancy)	0,0,0 (0.333)	0,0,0 (0.50)	0,0,0 (0.75)
Mo position (occupancy)	0,0,0 (0.667)	0,0,0 (0.50)	0,0,0 (0.25)
Profile function	pseudo-Voigt	pseudo-Voigt	pseudo-Voigt
Output Item/Parameter			
Cell parameter (Å)	3.91440 (11)	3.91827 (11)	3.91240 (14)
Volume ($Å^3$)	59.979	60.157	59.886
$D_{calc.}$ (g/cm^3)	13.082	16.097	19.039
Zero shift (° 2θ)	−0.0353 (32)	−0.1537 (52)	0.0464 (24)
No. obsd reflections	17	16	16
No. refined parameters	8	8	8
Scale factor ($\times 10^6$)	0.779 (4)	9.416 (17)	1.736 (3)
Profile parameter, **U**	0.299 (35)	−0.005 (93)	0.132 (26)
Profile parameter, **V**	0.149 (61)	2.19 (17)	0.163 (47)
Profile parameter, **W**	0.081 (20)	0.865 (55)	0.400 (15)
Profile parameter, η	0.891 (21)	1.344 (7)	1.0011 (74)
Profile parameter, $\overline{\mathbf{B}}_{iso}$	0.861 (16)	0.775 (11)	1.222 (12)
$\mathbf{R}_b$ (%); χ^2	0.494; 2.27	0.0488; 3.74	0.169; 1.67

0.4 mg/cm^2. Polarization measurements were performed galvanostatically. Current was varied manually with at least a 30-s stabilization period for each point recorded. Gas flow rates were changed with current to maintain constant stoichiometry (2 × stoichiometric). Long-term stability of the operating test fixture was not investigated.

RESULTS AND DISCUSSION

Complexes **1a**, **2a**, and **3a** were prepared to serve as single-source precursors of Pt–Mo/carbon nanocomposites having three different metal alloy stoichiometries. Each precursor complex is soluble in polar organic solvents and can be absorbed or deposited from solution onto commercial Vulcan carbon powder to give precursor/carbon composites of arbitrary metal loading. Reactive, thermal degradation of these precursor/carbon composites under oxidizing then reducing conditions affords the

corresponding $PtMo_2$(**1b**), PtMo (**2b**), or Pt_3Mo (**3b**)/carbon nanocomposites, as shown in equation (1). Products of precursor decompositions have not been identified. Total metal content of the final Pt–Mo/carbon nanocomposites **1b**, **2b**, and **3b** are 58 wt%, 43 wt%, and 29 wt%, respectively, as determined from bulk commercial elemental analysis.

Nanocomposite **1b** is prepared from a precursor/carbon composite containing the known (2*Pt–Mo*) trinuclear organometallic complex **1a** as precursor. Precursor **1a** is deposited on the carbon support in a single step and reactively degrades to Pt–Mo alloy upon heating the precursor **1a**/carbon composite in air to 280 °C followed by reduction in getter gas (1:9 H_2:N_2) at 650 °C and additional annealing at that temperature.

A bright-field TEM image, EDS spectrum, and XRD scan representative of nanocomposite **1b** are displayed in Fig. 1. Metal particles of high contrast and high dispersion are evident in the TEM micrograph. Metal particle sizes range in size from 1–10 nm, and the calculated average diameter (esd) is 3.5 (2.8) nm. The EDS spectrum shows emission from Pt and Mo with relative intensities corresponding to a Pt/Mo atomic ratio of 0.4 consistent within experimental precision to the Pt/Mo atomic ratio of 0.5 of precursor **1a**. The Pt:Mo atomic ratio determined from chemical bulk elemental analysis is 0.50. SAD electron diffraction patterns of nanocomposite **1b** clearly reveal five rings having the following observed *d*-spacings (Å) and Miller index assignments (*hkl*) based on a expected fcc unit cell symmetry: 2.16 (*111*); 1.90 (*200*); 1.32 (*220*); 1.13 (*311*); and 0.83 (*420*).

A XRD scan of nanocomposite **1b** as-prepared and as manipulated in ambient atmosphere reveals a predominant fcc pattern of peaks consistent with that expected for a Pt–Mo alloy having a fcc cell constant of 3.917 (1) Å. Peaks associated with this alloy phase are identified by the appropriate Miller indices. Scherrer's analysis of experimentally measured XRD peak widths for nanocomposite **1b** gives an average crystalline domain size of 12 (2) nm for the alloy nanoparticles that is significantly greater than the number-average particle size determined by TEM. This nanocomposite probably contains some number of atypically large alloy particles (vide infra).

A second pattern of diffraction peaks (indicated by asterisks in Fig. 1) of very weak intensity is also observed in the XRD scan of nanocomposite **1b**. This diffraction pattern is consistent with the formation of small amounts of phase-separated MoO_2 (ICDD card # 32-0671) and possibly Mo_2N (ICDD card #24-0768) due to air oxidation of $PtMo_2$ nanoparticles.

The air-sensitivity of $PtMo_2$ nanoparticles has been confirmed via *in situ* XRD analysis. A XRD scan of as-prepared nanocomposite **1b** (Fig. 2, scan "a") following reduction by getter gas at 650 °C reveals the fcc pattern expected for a pure Pt–Mo alloy product phase. The observed broad diffraction peaks indicate initial formation of very small particles. Annealing

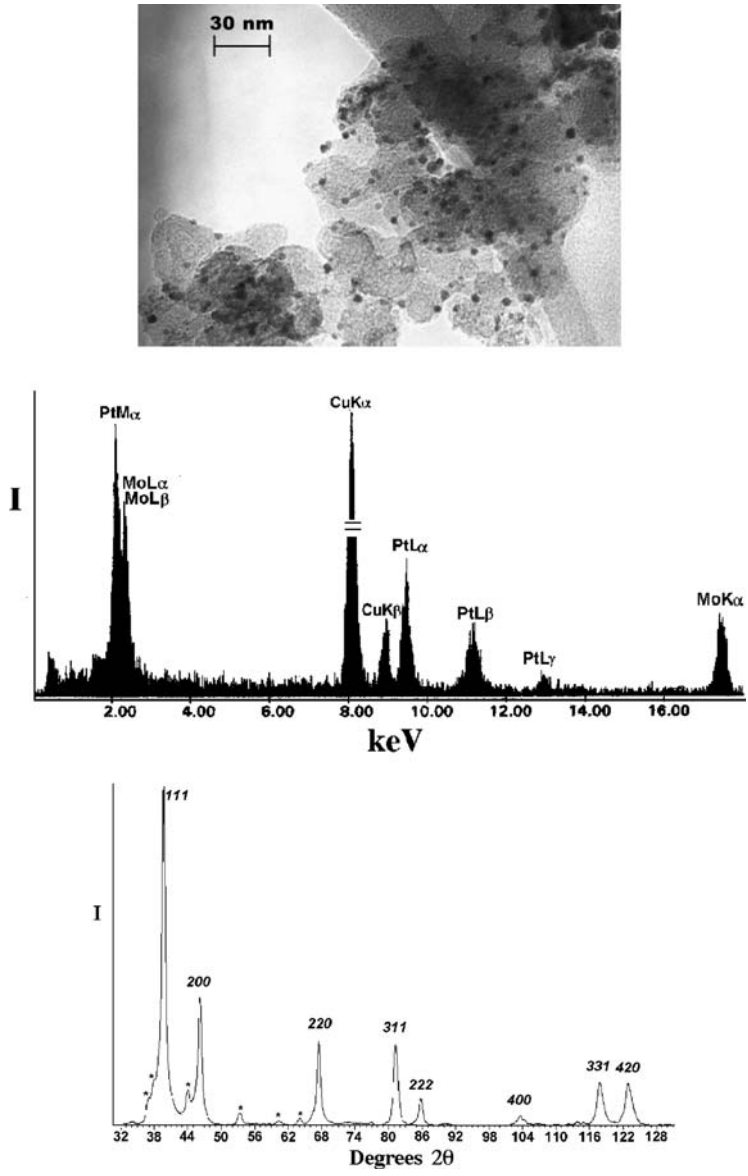

Fig. 1. Bright-field TEM image (top), EDS spectrum (middle), and powder XRD scan (bottom) of the $PtMo_2$/GCNF nanocomposite **1b**.

this sample for 50 min at 650 °C under nitrogen gives larger metal alloy nanocrystals and correspondingly sharper diffraction peaks (Fig. 2, scan "b"). A trace amount of Mo_2N is evident in this scan presumably due to reaction with N_2. When this sample is heated to 350 °C in air, two phases are clearly evident (Fig. 2, scan "c"). The pattern of peaks labeled as "P" is consistent with a fcc unit cell of lattice constant 3.923 Å and is assigned to a pure Pt metal phase (a = 3.9231 Å). The second diffraction pattern, peaks labeled as "M," is consistent with the known diffraction pattern of MoO_2. $PtMo_2$ nanoparticles are air-sensitive, and essentially all of the Mo content of these alloy nanoparticles undergoes phase separation as MoO_2 under conditions of intentional air oxidation.

Nanocomposite **2b** is prepared from a precursor/carbon composite containing the known (*Pt–Mo*) dinuclear organometallic complex **2a** as precursor. Complex **2a** was deposited on Vulcan carbon powder using a two-cycle deposition/degradation protocol and was reactively degraded by heating the precursor/carbon composite in air to 280 °C followed by

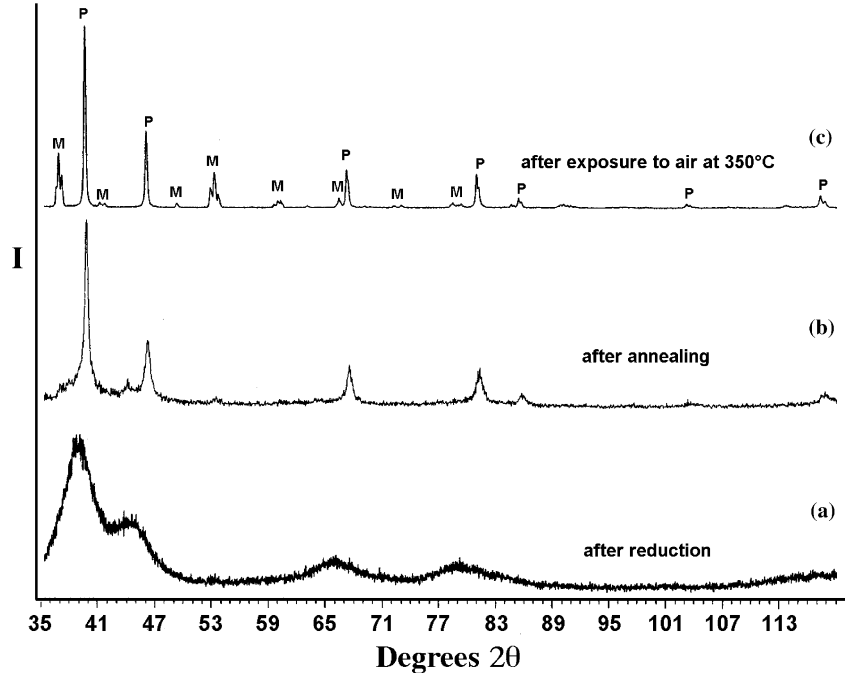

Fig. 2. *In situ* XRD analysis of the transformation of precursor **1a**/carbon composite to nanocomposite **1b** following initial reduction with getter gas at 650 °C (a), after annealing under N_2 at 650 °C (b), and after exposure to air at 350 °C (c).

reduction in getter gas (1:9 H_2:N_2) at 650 °C and additional annealing at that temperature.

A bright-field TEM image, EDS spectrum, and XRD scan representative of nanocomposite **2b** are displayed in Fig. 3. Metal particles exhibiting high contrast and high dispersion on the carbon powder support are evident in the TEM micrograph. Metal nanoparticle diameters range from 1 to 12 nm with a calculated average diameter (esd) of 3.8 (2.5) nm. The EDS spectrum shows emission from Pt and Mo with relative intensities corresponding to a Pt/Mo atomic ratio of 1.02 on the micron scale consistent within experimental precision to the 1:1 Pt/Mo atomic ratio of precursor **2a**. The Pt/Mo atomic ratio of nanocomposite **2b** determined by bulk chemical elemental analysis is 0.9.

A XRD scan of nanocomposite **2b** displays a fcc pattern of peaks consistent with the expected pattern of a Pt–Mo alloy having a fcc cell constant of 3.924 (5) Å. Peaks associated with this alloy phase are identified by the appropriate Miller indices. Scherrer's analysis of experimentally measured XRD peak widths for nanocomposite **2b** gives an average crystalline domain size of 3.9 (0.2) nm for the alloy nanoparticles consistent with the number-average particle size measured directly from TEM images.

The formation of nanocomposite **2b** has been followed via *in situ* XRD analysis under controlled conditions of atmosphere and temperature (see scans "a"–"c" in Fig. 4). Scan "a" is obtained from a precursor **2a**/carbon powder sample after thermal treatments at 280 °C in air and at 650 °C under getter gas. Formation of essentially pure Pt–Mo/carbon nanocomposite is evident. The total metal loading of the sample at this point is estimated to be ca. 25 wt%. A second portion of precursor **2a** is then deposited onto this intermediate nanocomposite, and the heating protocol described above is repeated for a second cycle. The total metal loading of the product nanocomposite is now ca. 43 wt%, and the sample displays a more intense diffraction pattern (scan "b"). Annealing this final nanocomposite at 650 °C under nitrogen for 1 h does not alter peak width significantly (scan "c"). In comparison to the one-step synthesis protocol used to prepare nanocomposite **1b**, the two-cycle deposition/degradation protocol used to prepare nanocomposite **2b** affords metal alloy nanocrystals less susceptible to thermally initiated particle growth. We speculate that a multi-cycle deposition protocol affords more uniform dispersion of precursor and of the resulting metal nanoparticles.

Nanocomposite **3b** is prepared from a precursor/carbon composite containing the (3 *Pt–Mo*)–(3 *Pt–Pt*) tetranuclear organometallic complex, **3a**, as precursor. Complex **3a**, or its $[PF_6]^-$ analogue, **3a′**, are new members of a known series of tetranuclear Pt_3M complexes prepared by reaction of organometallic anions with salts of $[Pt_3(\mu_3\text{-CO})\ (dppm)_3]^{2+}$ [5, 16]. Crystals

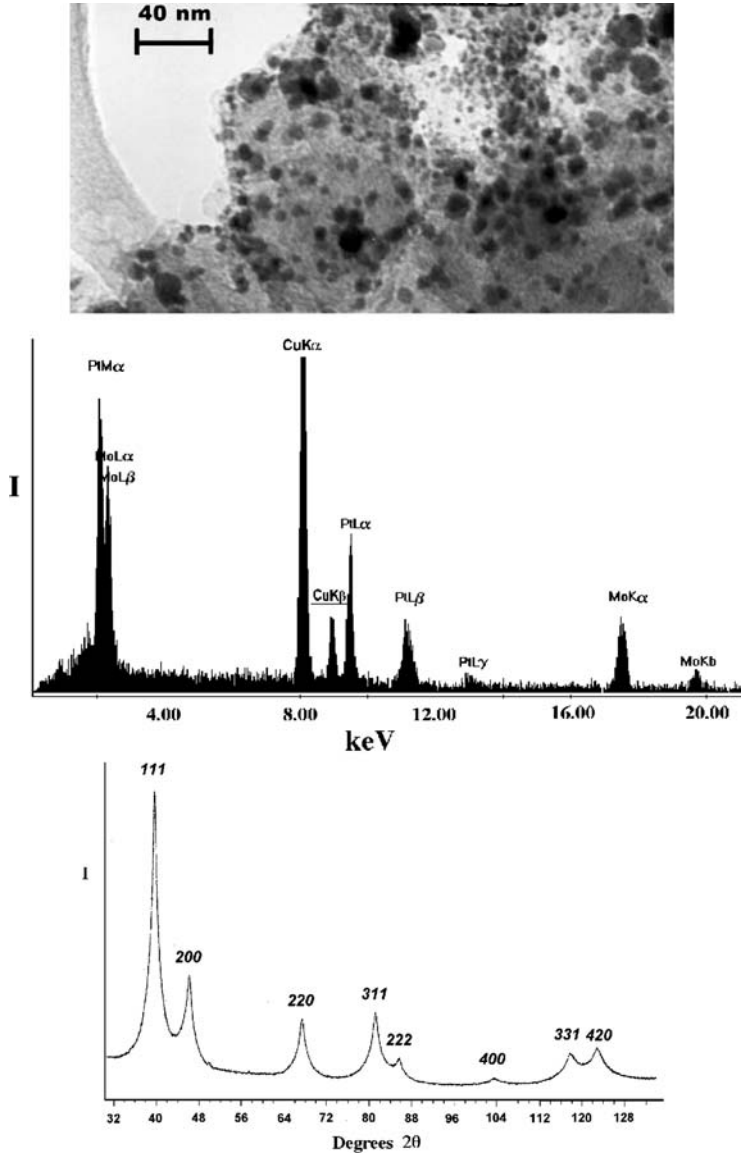

Fig. 3. Bright-field TEM image (top), EDS spectrum (middle), and powder XRD scan (bottom) of the PtMo/GCNF nanocomposite **2b**.

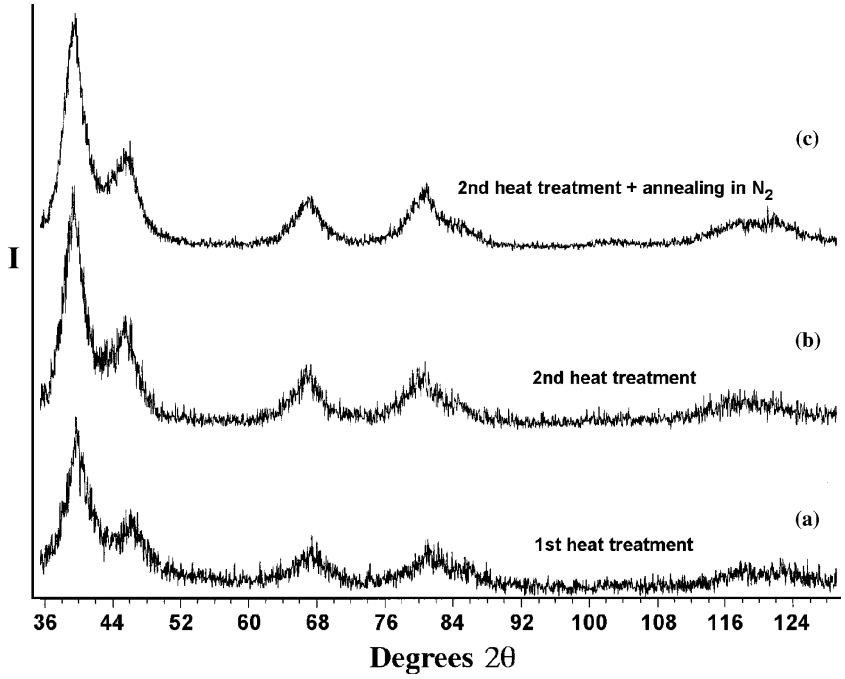

Fig. 4. *In situ* XRD analysis of the transformation of precursor **2a**/carbon composite to nanocomposite **2b** following an initial cycle of air oxidation at 280 °C and subsequent reduction with getter gas at 650 °C (a), after repeating this procedure for a second portion of precursor (b), and following annealing under N_2 at 650 °C (c).

of **3a** or **3a′** are mildly air sensitive. Solutions of these complexes degrade sufficiently rapidly that ^{31}P NMR data could be obtained only for complex **3a′**. Complexes **3a** and **3a′** are 54-electron cluster complexes, like the known $Mn(CO)_3$ and $Re(CO)_3$ analogues [16]. Commercial elemental microanalysis of crystals of **3a** or **3a′** give satisfactory results consistent with the compositions shown. A C–O stretching band for the μ_3-CO ligand is observed at 1712 cm^{-1} in the IR spectrum. ^{1}H-NMR spectra exhibit singlet resonances for the C_5H_5 ligand (δ4.79,**3a**; δ5.42, **3a′**) and the ^{31}P-NMR spectrum of complex **3a′** reveals the expected heptet resonance for the PF_6^- counterion and a dppm phosphorus resonance consistent with the isotopomer pattern expected for a $Pt_3(dppm)_3$ structural fragment (δ−8.3, $^1J_{PtP}$ = 3734 Hz; $^3J_{PP}$ = 196 Hz) [5, 16]. Corresponding ^{31}P-NMR spectral parameters for the analogous $[Pt_3(dppm)_3\ Mn(CO)_3][PF_6]$ complex are (δ−5.4,$^1J_{PtP}$ = 3030 Hz; $^3J_{PP}$ = 160 Hz) [16].

Precursor **3a** was deposited and degraded on Vulcan carbon powder using a two-cycle deposition/degradation protocol. Degradation conditions include heating precursor **3a**/carbon composites in air to 350 °C, reduction in getter gas (1:9 H_2:N_2) at 650 °C followed by an additional thermal treatment in air at 350 °C (vide infra).

A bright-field TEM image, EDS spectrum, and XRD scan representative of nanocomposite **3b** are displayed in Fig. 5. Metal particles of high contrast and widely dispersed on the carbon powder support are evident. Metal particle diameters range from 1 to 10 nm with a calculated average diameter (esd) of 3.4 (1.7) nm. The EDS spectrum shows emission from Pt and Mo with relative intensities corresponding to a Pt/Mo atomic ratio of 2.97 consistent within experimental precision to the 3:1 Pt/Mo atomic ratio of precursor **3a**. The Pt/Mo stoichiometry of nanocomposite **3b** determined by bulk chemical elemental analysis is 2.9.

A XRD scan of nanocomposite **3b** displays a fcc pattern of peaks having a cell constant of 3.9130 (8) Å. Peaks associated with this alloy phase are identified by the appropriate Miller indices. Scherrer's analysis of experimentally measured XRD peak widths for nanocomposite **2b** gives an average crystalline domain size of 4.6 (0.2) nm for the alloy nanoparticles consistent with the average particle size determined directly from TEM images.

Incorporation of an additional oxidation treatment in the synthesis of nanocomposite **3b** is required to prevent metal phosphide formation as confirmed via *in situ* XRD analysis (see scans "a"–"e" of Fig. 6). Heating precursor **3a**/Vulcan powder composites under air to 350 °C followed by reduction under getter gas at 650 °C produces an intermediate nanocomposite containing ca. 15 wt% total metal and two crystalline phases. A relatively small amount of the expected Pt–Mo alloy is formed along with a preponderance of the known binary metal phosphide, PtP_2, whose diffraction peaks (ICDD card # 3-1204) are identified by asterisks (Fig. 6, scan "a"). Deposition of a second portion of precursor **3a** followed by thermal treatment under air to 350 °C gives an intermediate nanocomposite ca. 29 wt% total metal showing no evidence of crystalline PtP_2 and the presence of broad diffraction peaks as expected for very small particles of a Pt–Mo alloy phase (Figure 6, scan "b"). Heating this intermediate nanocomposite under getter gas to 650 °C leads to reappearance of the PtP_2 phase (Fig. 6, scan "c"). Apparently, air oxidation induces phase separation of Pt and P, but amorphous phosphorus oxide material is still sufficiently present in the sample to reform PtP_2 upon reduction at high temperature. Subjecting this intermediate nanocomposite to yet a third oxidation cycle in air at 350 °C gives evidence of only a Pt–Mo alloy phase (Fig. 6, scan "d"). Brief reduction under getter gas produces the final nanocomposite consisting of

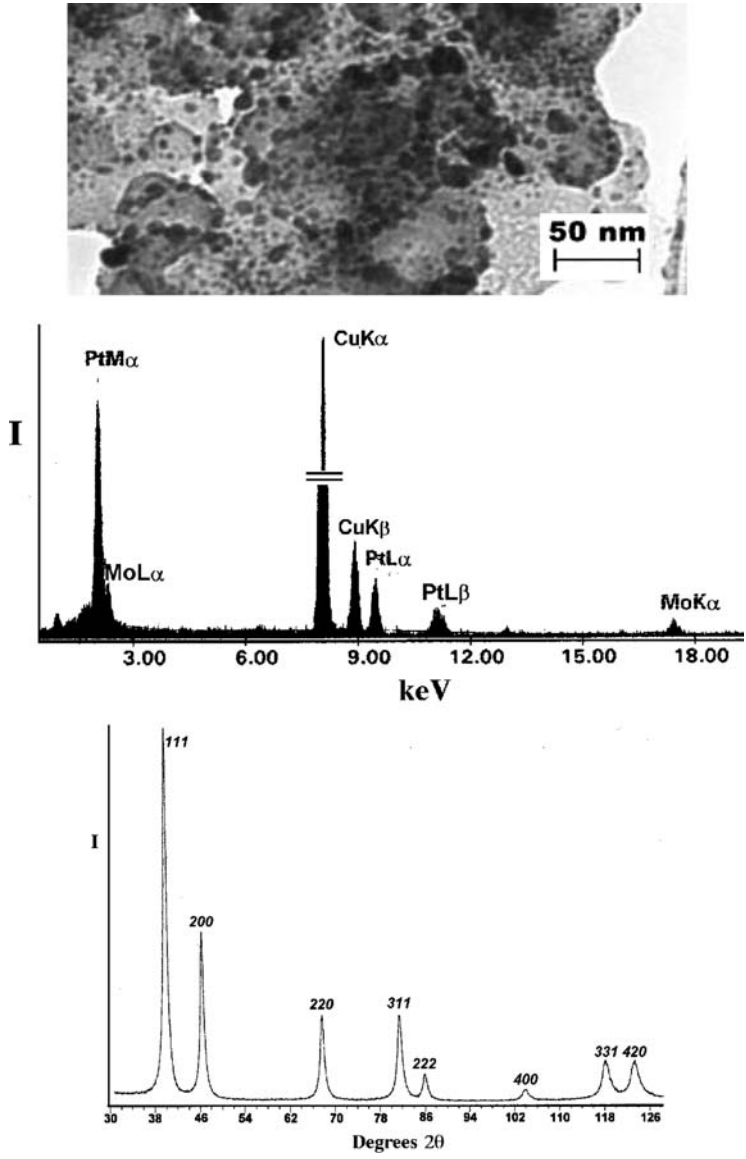

Fig. 5. Bright-field TEM image (top), EDS spectrum (middle), and powder XRD scan (bottom) of the Pt_3Mo/GCNF nanocomposite **3b**.

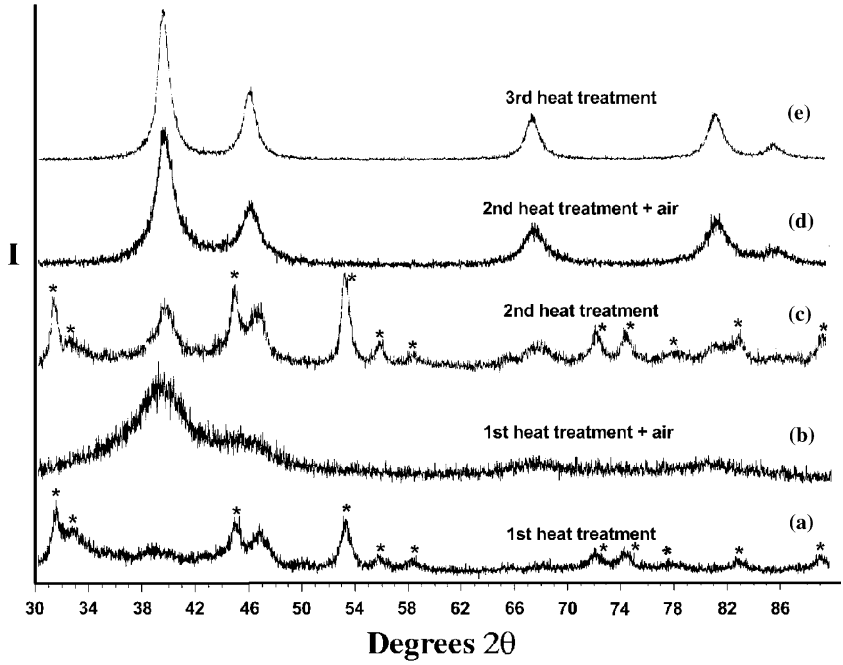

Fig. 6. *In situ* XRD analysis of the transformation of precursor **3a**/carbon composite to nanocomposite **3b** following initial air oxidation at 350 °C and subsequent reduction under getter gas at 650 °C showing formation of PtP_2 (a), following deposition of a second portion of precursor and air oxidation at 350 °C showing disappearance of PtP_2 (b), following reduction under getter gas at 650 °C showing re-appearance of PtP_2 (c), following air oxidation at 350 °C showing disappearance of PtP_2 (d), and following reduction under getter gas at 650 °C giving nanocomposite **3b** (e).

only the expected Pt_3Mo phase (Fig. 6, scan "e"). Bulk chemical elemental analysis indicates retention of phase-separated phosphorus (6.91 wt%) in the final nanocomposite **3b**. Although the speciation of this residual phosphorus content has not been determined experimentally, metal phosphide formation is not observed by XRD in the final nanocomposite. Precursors **1a** and **2a** lack phosphorus, so formation of PtP_2 in the syntheses of nanocomposites **1b** and **2b** is not a possible complication.

Unfortunately, Pt–Mo alloy compositions cannot be determined from experimentally measured lattice constants through application of Vegard's law due close similarity in the atomic radii of Pt and Mo (1.387 Å and 1.363 Å, respectively). As shown in Table II, lattice constants reported for Pt_xMo_y alloys prepared by various methods having Mo contents ranging from 5 to 43 atomic percent show little variation. Analysis of the XRD scans

of nanocomposites **1b**–**3b** using the indexing programs, TREOR [12] and DIVOL91 [13], confirms that these experimental diffraction patterns are consistent with Pt–Mo alloys having fcc unit cells and the cell constants reported above. In addition, each XRD scan was subjected to full-profile Rietveld analysis using FULLPROF software, as described in the Experimental section. Although unit cell lattice constants for nanocomposites **1b**–**3b** have been refined to high statistical precision, all three values fell within the range of 3.915 ± 0.003 Å.

The $PtMo_2$ and Pt_3Mo nanocomposites (**1b** and **3b**, respectively) are less than ideal materials for catalyst development because of the air sensitivity of nanocomposite **1b** and the complex precursor synthesis required for the preparation of nanocomposite **3b**. The PtMo nanocomposite **2b** lacks these disadvantages and was evaluated for CO tolerance as an anode electrocatalyst in a working H_2/O_2 PEMFC. Steady-state polarization measurements were carried out in a fuel cell test station using a cell fixture fitted for a 5-cm^2 MEA [15]. Cell performance of H_2/CO [0 ppm or 100 ppm]//O_2 fuel cells were measured at 85 °C using a Nafion 115 membrane and either nanocomposite **2b** or a commercial Pt/carbon nanocomposite as anode catalyst at a loading of 0.4 mg total metal/cm^2. A commercial Pt/C nanocomposite served as the cathode catalyst at the same metal loading.

Polarization curves recorded under the conditions stated above are shown in Fig. 7(a). The corresponding anode half-cell polarization plots are provided in Fig. 7(b). Both plots show similar behavior for nanocomposite **2b** and a commercial Pt/C catalyst as anode catalysts under H_2. These results are consistent with previous data comparing the steady-state anode

Table II. Lattice Spacings, a, Reported for Pt–Mo Solid Solutions Having a Face-Centered-Cubic Structure

Atomic % Mo	a [in Å]	Reference
5.0	3.912	[17]
9.6	3.907	[17]
18.4	3.909	[17]
20.0	3.91	[4b, c]
25.0	3.91	[4c]
25.0	3.908	[4e]
26.6	3.908	[17]
29.8	3.911	[17]
33.8	3.908	[17]
37.9	3.908	[17]
37.9	3.912	[17]
42.9	3.915	[17]

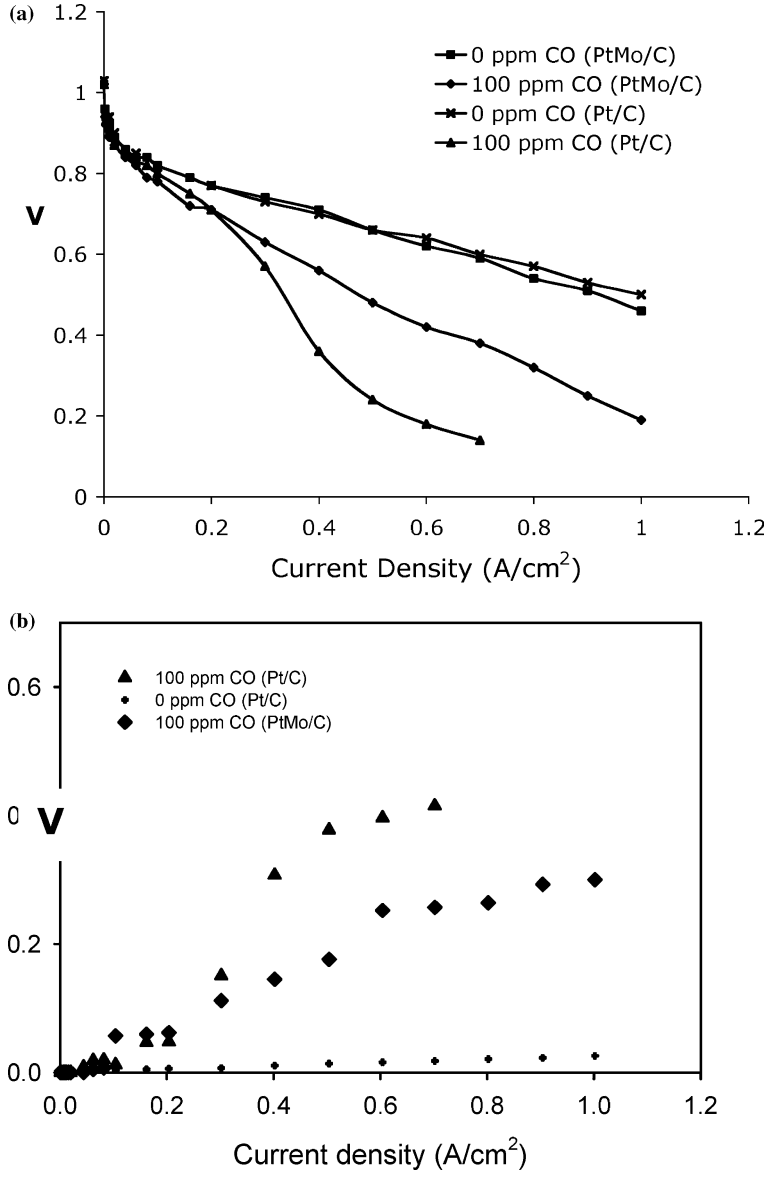

Fig. 7. Current density – voltage (V) PEMFC polarization curves (a) and anode half-cell polarization curves (b) comparing the performance of nanocomposite **2b** to that of a commercial Pt/C catalyst at the same total metal loading using either pure H_2 or H_2 containing 100 ppm CO as fuel.

polarization behavior of similar nano-dispersed Pt and alloys of Pt with the first-row transition series metals Cr–Ni [18]. Detailed analysis of electrode kinetic data including comparison of the activation energies reveals negligible differences in the activity of hydrogen oxidation as a consequence of alloying [18]. Differences in single-cell polarization are almost entirely due to differences in the electrocatalytic activity for CO oxidation on the different electrocatalyst surfaces, as shown in the half-cell polarization data plotted in Fig. 7(b).

However, when using H_2 containing 100 ppm CO as fuel, nanocomposite **2b** exhibits significant CO-tolerance relative to the performance recorded for the commercial Pt/C anode catalyst. Anode overpotential losses with 100 ppm CO in H_2 fuel at a current density of 500 mA/cm^2 [see Fig. 7(b)] for nanocomposite **2b** is 0.16 V compared to 0.36 V for the Pt/C catalyst, giving a potential difference of 200 mV. Though the CO-tolerance observed for nanocomposite **2b** is less than that reported for a 4:1 PtMo/C catalyst, it is comparable to the CO-tolerance measured for 1:1 PtRu/C catalysts [4]. Given that cost efficiencies could be gained by using Mo instead of Ru, these test results are encouraging. Further study of the PEM CO-tolerance of nanocomposite **2b**, or of related PtMo/C catalysts prepared by the synthesis strategy, appears to be warranted.

ACKNOWLEDGMENTS

Research support provided by the U.S. Army Research Office under grant numbers DAAH04-95-1-0146, DAAH04-96-1-0179, DAAH04-96-1-0302 and DAAG55-98-1-0362 is gratefully acknowledged by C.M.L.

REFERENCES

1. (a) E. Antolini (2003). *Mater. Chem. Phys.* **78**, 563. (b) M. P. Hogarth and T. R. Ralph (2002). *Platinum Metals Rev.* **46**, 146. (c) T. R. Ralph, and M. P. Hogarth (2002). *Platinum Metals Rev.* **46**, 117. (d) A. Hamnett (1997). *Catal. Today* **38**, 445. (e) M. P. Hogarth, and G. A. Hards (1996). *Platinum Metals Rev.* **40**, 150. (f) G. K. Chandler, J. D. Genders, and D. Pletcher (1997). *Platinum Metals Rev.* **41**, 54. (g) T. R. Ralph (1997). *Platinum Metals Rev.* **41**, 102. (h) A. Hamnett, and G. L. Troughton (1992). *Chem. Ind.* 480.
2. (a) W. D. King, E. S. Steigerwalt, G. A. Deluga, J. D. Corn, D. L. Boxall, J. T. Moore, D. Chu, R. Jiang, E. A. Kenik, and C. M. Lukehart, *in* B. Zhou, S. Hermans and G. A. Somorjai, (eds.), *Nanotechnlogy in Catalysis*, Vol. 1, (Kluwer Academic/Plenum Publishers, New York, NY, USA, 2004) Chapter 10. (b) W. D. King, J. D. Corn, O. J. Murphy, D. L. Boxall, E. A. Kenik, K. C. Kwiatkowski, S. R. Stock, and C. M. Lukehart (2003). *J. Phys. Chem. B* **107**, 5467. (c) E. S. Steigerwalt, G. A. Deluga, and C. M. Lukehart (2002). *J. Phys. Chem. B* **106**, 760. (d) E. S. Steigerwalt, G. A. Deluga, D. E. Cliffel, and C. M. Lukehart (2001). *J. Phys. Chem. B* **105**, 8097. (e) D. L. Boxall, G. A. Deluga, E. A. Kenik, W. D.King, and C. M. Lukehart (2001). *Chem. Mater.* **13**, 891. (f)

D. L. Boxall, E. A. Kenik, and C. M. Lukehart (2001). *Mater. Res. Soc. Sym. Proc.* **589**, 265. (g) C. M. Lukehart, D. L. Boxall, J. D. Corn, M. Hariharasarma, W. D. King, K. C. Kwiatkowski, E. S. Steigerwalt, and E. A. Kenik (1999). *ACS Fuel Chem. Div. Preprints* **44**, No. 4,982. (h) D. L. Boxall, C. M. Lukehart, E. A. Kenik (1999). *Proc. ASME Advanced Energy Systems Div.* **39**, 327.

3. S. J. Lee, S. Mu kerjee, E. A. Ticianelli and J. McBreen (1999). *Electrochim. Acta.* **44**, 3283.
4. (a) A. Pozio, L. Giorgi, E. Antolini, and E. Passalacqua (2000). *Electrochim. Acta* **46**, 555. (b) S. Mukerjee, S. J. Lee, E. A. Ticianelli, J. McBreen, B. N. Grgur, N. M. Markovic, P. N. Ross, J. R. Giallombardo, and E. S. De Castro (1999). *Electrochem. Solid-State Lett.* **2**, 12. (c) B. N. Grgur, N. M. Markovic, and P. N. Ross (1999). *J. Electrochem. Soc.* **146**, 1613. (d) B. N. Grgur, N. M. Markovic, and P. N. Ross (1998). *J. Phys. Chem.* **B 102**, 2494. (e) B. N. Grgur, G. Zhuang, N. M. Markovic, and P. N. Ross (1997). *J. Phys. Chem.* **B 101**, 3910.
5. I. G. Ferguson, B. Lloyd and R. J. Puddephatt (1986). *Organometallics.* **5**, 344.
6. T. S. Piper and G. Wilkinson (1956). *J. Inorg. Nucl. Chem.* **3**, 104.
7. H. C. Clark and L. E. Manzer (1973). *J. Organometal. Chem.* **59**, 411.
8. G. B. Kauffman (1963). *Inorg. Synth.* **7**, 251.
9. A. Fukuoka, T. Sadashima, I. Endo, N. Ohashi, Y. Kambara, T. Sugiura, K. Miki, N. Kasai and S. Komiya (1994). *Organometallics.* **13**, 4033.
10. (a) P. Braunstein, and J. Dehand (1970). *J. Organometal. Chem.* **24**, 497. (b) R. G. Hayter (1963). *Inorg. Chem.* **2**, 1031.
11. H. P. Klug and L. E. Alexander, *X-ray Diffraction Procedures for Polycrystalline and Amorphus Materials*, 2nd ed., (John Wiley & Sons, New York, 1974).
12. P. E. Werner, L. Eriksson and M. Westdahl (1985). *J. Appl. Cryst.* **18**, 367.
13. (a) D. Louer, and M. Louer (1972). *J. Appl. Cryst.* **5**, 271. (b) A. Boultif, and D. Louer (1991). *J. Appl. Cryst.* **24**, 987.
14. J. Rodriguez-Carvajal (1997). *Program FULLPROF*, version 3.3, August 1997, ILL.
15. S. J. Lee, S. Mukerjee, J. McBreen, Y. W. Rho and T. H. Lee (1998). *Electrochim. Acta.* **43**, 3693.
16. J. Xiao, E. Kristof, J. J. Vittal and R. J. Puddephatt (1995). *J. Organometal. Chem.* **490**, 1.
17. W. A. Pearson, *Handbook of Lattice Spacings and Structures of Metals and Alloys* (Pergamon Press, Oxford, UK, 1958), pp. 755.
18. S. Mukerjee and J. McBreen (1996). *J. Electrochem. Soc.* **143**, 2285.